Basins of attraction in forced systems with time-varying dissipation

James A. Wright[1], Jonathan H.B. Deane[1], Michele Bartuccelli[1], Guido Gentile[2]

[1]Department of Mathematics, University of Surrey, Guildford, GU2 7XH, UK
[2]Dipartimento di Matematica e Fisica, Università di Roma Tre, 00146 Roma, Italy
Email: j.wright, j.deane, m.bartuccelli@surrey.ac.uk, gentile@mat.uniroma3.it

Abstract

We consider periodically forced systems with dissipation depending on time and study how the sizes of the basins of attraction are modified with respect to the case of constant dissipation. In particular, we investigate cases in which having information as to how the system behaves for constant dissipation may be used when dissipation varies over a certain time interval before settling at a constant final value. First, we consider situations where one is interested in the basins of attraction for damping coefficients growing linearly between two given values, in the time interval where it varies, for a large number of choices of the interval: we outline a method to reduce the computation time required to estimate numerically the relative areas of the basins for all values of the time interval, and discuss its range of applicability. Second, we observe that sometimes very slight changes in the time interval may produce abrupt large variations in the relative areas of the basins of attraction of the surviving attractors: we show how comparing the contracted phase space at a time after the final value of dissipation has been reached with the basins of attraction corresponding to that value of constant dissipation can explain the presence of such variations. Both procedures are illustrated by application to a pendulum with periodically oscillating support.

Keywords: attractors, basins of attraction, forced systems, dissipative systems, damping coefficient, non-constant dissipation, pendulum with oscillating support.

1 Introduction

Dissipative forced mechanical systems are widely studied in the literature. Usually the dissipation is considered to be constant, even though, on physical grounds, one expects it to increase in time, because of several effects, such as ageing, cooling, general wear and build up of dirt. Of course, if one is interested in dynamics over short or medium times, the constant approximation is adequate for a correct description of the motion. On the other hand, if one needs to investigate systems evolving on very large time intervals, taking into account the time-dependence of the dissipation becomes a very important issue, as it may radically change the asymptotic behaviour of the system. Classical examples where such a phenomenon appears naturally arise in celestial mechanics, when one is interested in the evolution of planets or satellites over times which can be up to the order of billions of years — that is greater than their solidification time [1, 2]. In that case, the dissipation is virtually zero when the celestial body starts forming, and thereafter it slowly increases towards a limit value which is reached asymptotically, so that after some point it can be assumed to be constant for all practical purposes [3, 4, 5, 6]; we refer to [7, Appendix E] for a more detailed discussion. A paradigmatic case, of intrinsic physical interest and at the same time simple enough to be studied

in detail both numerically and analytically, is the so-called spin-orbit model [8, 9]: because of the interplay between forcing and friction, a satellite orbiting around a planet is eventually captured in an "orbital resonance", such that the rotational period is rationally related to the orbital period. Usually the two periods are equal (synchronous resonance), with the remarkable exception of Mercury, which can be considered as a satellite of the Sun [8, 9, 10, 11]. The possible resonances are determined by the coexisting periodic attractors of the system and the probability of capture in a given attractor is related to the size of the corresponding basin of attraction [12, 13, 7, 14].

More generally, in any forced mechanical system subject to dissipation, the probability of capture in a given attractor can be studied by estimating the relative areas of the corresponding basins of attraction. This can be achieved numerically by considering a large sample of initial conditions and studying towards which attractor each of them evolves; note that usually investigations of dissipative systems are focused on the topology of the basins of attraction, whilst, in our case, the relevant property of the basins is the fraction of initial conditions belonging to them. However, the actual sizes of the basins can be influenced in a relevant way by the fact that the dissipation has increased during the time evolution of the system: considering only the final value would lead to wrong results [7]. Since the exact growth profile of dissipation as a function of time is not known in general, it may be important to compare several profiles in order to ascertain whether the final output remains more or less the same or, instead, drastically changes by taking a different profile. This has been investigated in detail in some special cases [7, 15], and the results were found to depend sensitively on the profile. Because of the large integration times and the numerous initial conditions that one has to consider in order to obtain reliable estimates of the sizes of the basins of attraction, a numerical study necessarily requires a lot of computer time; see [7, 14] for further comments. Therefore, a method to speed up the numerical computations when several profiles must be considered would be useful. In this paper, we address such a problem.

In the spin-orbit model, and indeed in many celestial mechanics problems, the values of the dissipation are very small and the time scales over which the phenomenon described above can be observed are very large. As a consequence the integration times are extraordinarily long and the numerical analysis presents very delicate issues, as pointed out in [14]; see also [16, 17]. Therefore, it is reasonable to consider first simpler models, such as the forced cubic oscillator or the pendulum with oscillating support, which have already been studied in [7, 15]. Of course, the latter can be viewed as toy models with respect to systems more relevant from a physical point of view, such as the aforementioned celestial mechanics problems. Nevertheless, by taking a simpler model and allowing larger values for the dissipation, we can reduce in an appreciable way the integration times — which are still large, but not so large as to require *ad hoc* strategies to complete a very large number of runs in a realistic time. This may lead us to reach conclusions and insights, which can obviously be useful before attacking more difficult numerical investigations.

For this reason, in this paper we consider explicitly the same model as studied in [15], that is the forced pendulum, with the damping coefficient varying linearly in time from an initial value γ_i to a final value γ_f, with both γ_i and γ_f fixed. If T_f denotes the full evolution time of the system and T_0 is the time after which the damping coefficient becomes identically equal to γ_f (hence T_0 is related to the growth rate of the damping coefficient), one may be interested in comparing with each other several values of T_0, say M of them. The evolution time T_f is in general very large: it has to be large enough for all trajectories to approach closely the corresponding attractors and hence one needs $T_f \gg 1/\gamma_f$, so a naive analysis would require a very long overall integration time of order of NMT_f, if N is the number of initial conditions. Of course, instead of taking T_f to be the same for all trajectories, a wiser choice would be to choose T_f depending on the initial conditions, but this would not really speed up the numerical simulations in an appreciable way (more details will be provided in Section 4.1). Here, we propose a method for the fast computation of the basins of attraction for all values of T_0 which we are interested in, which allows us to obtain the results after an overall integration time much shorter than NMT_f. As a byproduct of our analysis, we shall also be able to explain some striking behaviour of the system observed in [15].

The rest of the paper is organised as follows. In Section 2, we introduce the class of systems that we aim to investigate and briefly describe the main results of our analysis. In Section 3 we

provide a few preliminary definitions and introduce some basic tools, such as the movement map and the density map. In Section 4 we describe in detail the method of fast numerical computation of the basins of attraction: first we present a general formulation, then we implement the method in the special case of the pendulum with oscillating support and with damping coefficient linearly varying in time. In Section 5 we apply our analysis to explain the phenomenon observed in [15], that is the sudden appearance of peaks in the curves describing how the relative areas of the basins of attraction vary as functions of the growth rate of linearly increasing dissipation. Finally, in Section 6 we draw the conclusions and discuss ranges and limits of applicability of the method.

2 Model

Consider the ordinary differential equation

$$\ddot{\theta} + f(\theta, t) + \gamma(t)\,\dot{\theta} = 0, \tag{2.1}$$

where $\theta \in \mathbb{T} = \mathbb{R}/2\pi\mathbb{Z}$, the dots denote derivatives with respect to time t, the driving force f is smooth and 2π-periodic with respect to both its arguments and the damping coefficient $\gamma(t) \geq 0$ depends on time. For concreteness we shall consider explicitly the case of a pendulum with oscillating support, which is described by an ordinary differential equation of the form

$$\ddot{\theta} + \big(\alpha - \beta\cos t\big)\sin\theta + \gamma(t)\,\dot{\theta} = 0, \qquad \alpha, \beta \in \mathbb{R}, \tag{2.2}$$

but our results apply to systems (2.1) with more general forces, including the spin-orbit model with MacDonald's tidal torque [9], or even systems of the form $\ddot{x} + g(x, t) + \gamma(t)\,\dot{x} = 0$, with $x \in \mathbb{R}$, such as those considered in [7].

With a few exceptions, forced systems of the form (2.1) have been studied only in the case of constant dissipation. Despite the simplicity of the model, not much is known analytically. For instance only a finite set of attractors are expected to exist [18, 16, 17], but no proof is known for this. Furthermore, the corresponding basins of attraction are usually calculated only numerically; see for example [19, 20, 21, 22, 23, 24]. In addition to that, as argued in Section 1, in many physical systems it may not be legitimate to consider the damping coefficient to be constant throughout their entire evolution. Time-dependent dissipation has been studied in [7, 15], where the focus was mainly on the case of $\gamma(t)$ varying linearly over some initial time span, say $t \in [0, T_0]$, after which it remains constant. In that case, as discussed in the quoted papers, only considering the final value of the damping coefficient does not give a correct representation of the basins of attraction and the entire time evolution of $\gamma(t)$ must be taken into account. A somewhat similar situation is discussed in [25], where the authors consider a dissipative oscillator undergoing forcing which grows in amplitude until it reaches a fixed value: with a parameter increasing in time toward a final value, the asymptotic behaviour turns out to be strikingly different with respect to the case where the parameter is constant for all time.

Nevertheless, the analysis of a system with constant damping coefficient γ may provide information for the same system with damping coefficient varying in time. For constant γ, consider an attractor and denote by $A(\gamma)$ the relative area of the corresponding basin of attraction, that is the percentage of initial data in a given sample region whose trajectories go to that attractor. It has already been pointed out in [7, 15] that, if one knows the profiles $\gamma \mapsto A(\gamma)$ describing how the relative areas of the basins of attraction depend on γ in the system with constant dissipation, then, when $\gamma(t)$ varies quasi-statically (that is very slowly) from an initial value γ_i towards a final value γ_f over a time T_0 and thereafter remains constant, one may be able to predict the relative areas of the basins by looking only at the profiles, and the slower the variation of the damping coefficient, the better the prediction. More precisely, at least in the perturbation regime, if an attractor exists for $\gamma = \gamma_f$, then, for the system with $\gamma(t)$ increasing slowly towards the value γ_f, the relative area of the corresponding basin of attraction is close to the value that the function $A(\gamma)$ attains for $\gamma = \gamma_i$. Moreover, the larger T_0, the closer the relative area will be to this value.

In this paper, we want to discuss other cases, where knowledge of the behaviour of the system for constant γ may be used in the case in which dissipation changes in time. In particular, we shall discuss the following issues.

1. Suppose that one is interested in investigating systems with $\gamma(t)$ varying linearly from an initial value γ_i to a final value γ_f, with γ_i and γ_f fixed, over a time interval $[0, T_0]$, for many values of T_0, and then remains fixed at the value γ_f for the remaining time interval $[T_0, T_f]$, where T_f is the entire time evolution. The time T_f is the time over which one wants to study the system and has to be large enough for the attractors to be closely reached. In Section 4 we outline a method to speed up the computation of the basins of attraction. The method utilises basins of attraction calculated for the system with constant damping coefficient γ_f, and it reduces the length of time over which it is necessary for the equations of motion to be numerically integrated. In effect, our method is to extrapolate from an observation time $T_1 \geq T_0$ to the full evolution time T_f, by using pre-computed data: the smaller T_1 with respect to T_f, the larger reduction of computational time. We will refer to this as 'the method of fast numerical computation'. This is first stated as a general method and later numerically implemented for the pendulum with oscillating support.

2. In Section 5, we come back to a phenomenon observed in [15]. When the damping coefficient increases linearly over a time T_0 towards a final value γ_f, the relative areas of the basins of attraction of the surviving attractors most of time change smoothly as functions of T_0, without abrupt variations; however, in a few cases we observed sharp jumps, concentrated in small intervals of values of T_0 — see Figures 21 and 22 in [15]. By using the same ideas as in the method of fast numerical computation, we offer an explanation of why this happens.

The method of fast numerical computation can significantly reduce the computation time to calculate the basins of attraction when the number of values of T_0 to investigate is large, particularly for systems which require long time integration or where computationally heavy integration methods are needed. Assuming dissipation to increase with time is very natural from a physical point of view, as pointed out in the Introduction. A linear increase may seem less natural; however, in addition to being particularly well-suited for numerical investigation, it also simulates situations where dissipation tends to settle around some asymptotic value, which again are of physical interest; we refer to [7] for further comments. Therefore, in this paper we have focused on the linear case. Nevertheless we expect our results to apply in more general contexts, where the variation of the damping coefficient is not linear (or not even monotonic), or the final value is reached only asymptotically.

The results produced by the method of fast numerical computation show good agreement with the results obtained by integrating the system over the full time T_f required for trajectories to settle numerically on the persistent attractive solutions. We shall find not just that there are only small differences between the results obtained with the method of fast numerical computation and those of the full time integration, but also that these differences are less than the width of the 95% confidence interval on the results as computed by Monte Carlo simulation. However, as we shall see the choice of the observation time T_1 may be a delicate matter and need a few *caveats*. In particular the method can be of practical use only if T_1 can be taken appreciably smaller than the evolution time T_f. In general, the right choice of the parameter T_1 is something that has to be decided case by case; more comments on this will be given in Section 6.

3 Some preliminary definitions

In order to study the basins of attraction of a dissipative dynamical system $\dot{\boldsymbol{x}} = \boldsymbol{F}(\boldsymbol{x}, t)$ in $\mathbb{T} \times \mathbb{R}$, one takes initial conditions in a sample region of phase space, say $S \subset \mathbb{T} \times \mathbb{R}$, and lets them evolve in time. As a result of dissipation, the sample region S will contract with time as trajectories move towards the persisting attractors. This leads to the following definition.

Definition 1 *Given a dissipative dynamical system and a sample region S, the region of phase space still occupied by trajectories starting in S at time 0, after time T has elapsed, will be called the* contracted phase space *at time T and denoted by C_T.*

In principle S is arbitrary, but in practice it is convenient to take it in such a way that (a) it contains the (relevant) attractors and (b) one has $C_T \subset S$ for T large enough. Thus, if the total time over which the system evolves consists of two intervals, a first interval $[0, T_0]$ in which $\gamma = \gamma(t)$ varies and a second interval $[T_0, T_f]$ in which $\gamma = \gamma_f$ is constant, then whilst the first interval takes initial conditions from the whole of S, the second one only receives initial conditions from C_{T_0}.

It is sometimes useful to know to which points in C_T points in S are mapped. This information is captured in the movement map, which is defined as follows.

Definition 2 *Fix a set X_0 of points $\boldsymbol{x}_0 \in \mathbb{T} \times \mathbb{R}$ at time $t = 0$ and let X_1 be the set of corresponding points $\boldsymbol{x}_1$ that the trajectories with such initial conditions arrive at for $t = T$. The continuous, bijective map M_T defined by $M_T(X_0) = X_1$ is called a* movement map *from time 0 to time T.*

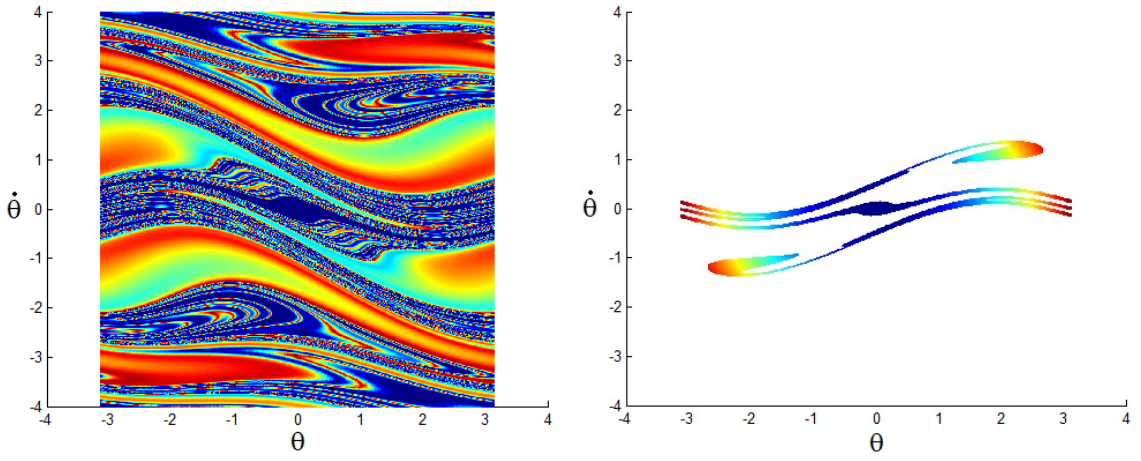

(a) (b)

Figure 1: An example of the effect of the movement map for (2.2), with $\alpha = -0.1$, $\beta = 0.545$ and $\gamma(t)$ growing linearly from $\gamma_i = 0.1$ to $\gamma_f = 0.2$ over time $T_0 = 8\pi$: (a) sample phase space S at time $t = 0$ and (b) contracted phase space $C_{8\pi}$. Colours are used to indicate subregions of S and $C_{8\pi}$: a trajectory starting in a region of S marked by a particular colour will arrive in a region of $C_{8\pi}$ with the same colour.

The contracted phase space need not (and in most cases will not) be uniformly populated. To specify how "dense" regions of the contracted phase space are we introduce the following definition.

Definition 3 *Let $r > 0$ be small enough. Given a dissipative dynamical system and a sample region S, let C_T be the contracted phase space at time T. Consider a cover of C_T with cubes of side r and denote by X the set of centres of the cubes. Fix $X_0 \subset S$ and for $\boldsymbol{x} \in X$ define $\rho(\boldsymbol{x})$ as the fraction of trajectories starting in X_0 which evolve into the cube of side r and centre $\boldsymbol{x}$ at time T. We define the* density map *from time 0 to time T as the map which associates the value $\rho(\boldsymbol{x})$ with each $\boldsymbol{x} \in X$.*

If $X_0 = S$, the function $\rho(\boldsymbol{x})$ is expected to become r-independent for r small enough; for this reason we have omitted its dependence on r. On the other hand, if X_0 is a discrete set (as in any numerical implementation), r cannot be too small for the definition to make sense.

The definitions above are given explicitly in $\mathbb{T} \times \mathbb{R}$, but could be easily extended to $\mathbb{R}^2$, or even to higher dimensional systems. Throughout the rest of the paper we focus on systems of the form (2.1), so that $\boldsymbol{x} = (\theta, \dot{\theta})$ and the driving force is 2π-periodic in t. Moreover we consider damping coefficients $\gamma(t)$ which vary linearly between two values and become constant after a time T_0. If

$X_0 \subset S$ is the set of initial conditions, we take $T_1 \geq T_0$ such that $X_1 = M_{T_1}(X_0) \subset C_{T_1} \subset S$. For the system (2.2), a convenient choice for the sample region S turns out to be $S = [-\pi, \pi] \times [-4, 4]$. When considering a trajectory $(\theta(t), \dot{\theta}(t))$, the points $\boldsymbol{x}_0 = (\theta(0), \dot{\theta}(0))$ and $\boldsymbol{x}_1 = (\theta(T_1), \dot{\theta}(T_1))$ are just different points on the same trajectory and share the same path as $t \to \infty$. Furthermore, if $T_1 = 2N\pi$, where $N \in \mathbb{N}$, since the forcing is 2π-periodic then the solutions with initial conditions $\boldsymbol{x}_0$ and $\boldsymbol{x}_1$ at time $t = 0$ move towards the same attractor if we set $\gamma = \gamma_f$ from $t = 0$. This observation will be used when choosing T_1 to be a multiple of 2π in the following — see Section 4.1.

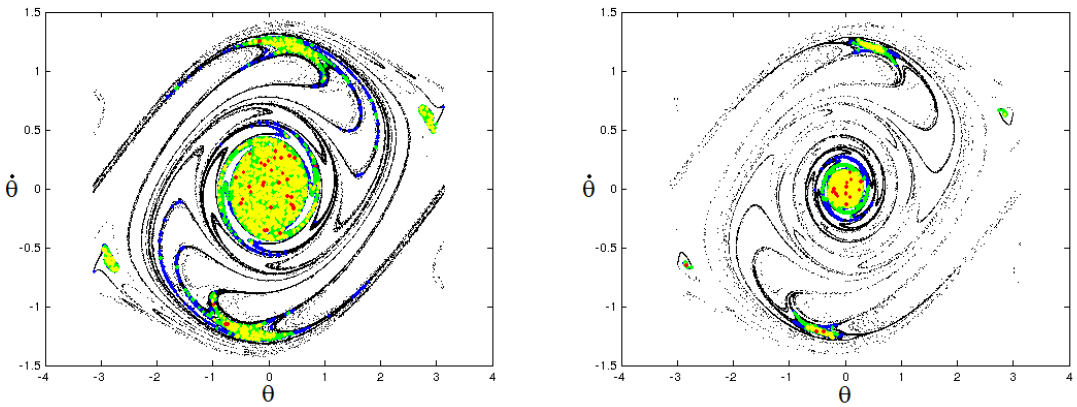

(a) (b)

Figure 2: Contracted phase space for (2.2), with $\alpha = 0.5$, $\beta = 0.1$ and $\gamma(t)$ decreasing linearly from $\gamma_i = 0.05$ to $\gamma_f = 0.02$ over a time (a) $T_0 = 32\pi$ and (b) $T_0 = 48\pi$. The densities are coded with red being the most dense, then yellow, green, blue and black.

A discrete approximation to the movement map will be represented by a $p \times m$ matrix, in which the indices $i = 0, \ldots, p$ and $j = 0, \ldots, m$ correspond to the coordinates of the initial condition $(\theta_0 = -3.14 + i\Delta\theta, \dot{\theta}_0 = -4 + j\Delta\dot{\theta})$, with $p\Delta\theta = 6.28$ and $m\Delta\dot{\theta} = 8$, and in each i,j-th entry is a vector of the coordinates $(\theta_1, \dot{\theta}_1)$ for the corresponding trajectory at time T_1. We can represent the action of the movement map using a colour code for the phase space as shown in Figure 1: in this way, we can follow how different regions evolve in time. A numerical representation of a density map can be achieved by rounding trajectories onto a grid, as done for the movement map. Different colours may be used to express how dense regions of phase space are. In particular a density map allows us to see how the most dense regions of the contracted phase space move with variations in T_0 — see Figure 2: different colours correspond to regions with a different density of trajectories at the observation time.

4 Fast numerical computation of the basins of attraction

In Section 4.1 we first describe the method of fast numerical computation *in abstracto*, then, in Section 4.2, we explicitly discuss the pendulum with oscillating support described by (2.2).

4.1 General setting

We are interested in investigating a system of the form (2.1) with $\gamma(t)$ varying in time from an initial value γ_i to the final value γ_f over a time T_0. The basins of attraction can be obtained as follows. One covers the sample region S with a mesh of points, with the requirement that the limiting solution of each point on the mesh is known for constant $\gamma = \gamma_f$. Concretely, this means that the basins of attraction of the system (2.1) with constant $\gamma(t) = \gamma_f$ are already known. In general, this information can only be obtained numerically and requires integration of the equations

of motion for a time large enough for the attractors to be closely approached. The easiest way to proceed is to take the same integration time T_f for all initial conditions, say $T_f = \Delta/\gamma_f$, where $\Delta > 0$ is sufficiently large. Actually $\Delta = 60$ (or even less) turns out to be enough for all trajectories to have reached a small neighbourhood of the corresponding attractors, when the latter are well separated in phase space, as in the cases considered below — as well as in [26, 7, 15]. To reduce the overall integration time, one can choose, for each trajectory, an integration time depending on its initial condition $\boldsymbol{x}$, that is to fix $T_f(\boldsymbol{x})$ in such a way that the trajectory with initial condition $\boldsymbol{x}$ has reached any attractor with a pre-assigned tolerance value. Then, the overall integration time for a set of initial conditions $\boldsymbol{x}_k$, with $k = 1, \ldots, N$, will be $N\overline{T}_f$, with

$$\overline{T}_f := \frac{1}{N} \sum_{k=1}^{N} T_f(\boldsymbol{x}_k), \tag{4.1}$$

which is smaller than the previously defined T_f, by definition. However, at least in the class of models that we have investigated, the distribution of integrations times turns out to be very peaked around $\overline{T}_f$, which in turn is not much smaller than the maximum value that $T_f(\boldsymbol{x})$ can reach by varying the initial condition $\boldsymbol{x}$; more quantitative details will be given below.

Then, we consider the system (2.1) with $\gamma(t)$ varying toward the final value γ_f over a time T_0 much smaller than T_f. We would like to obtain the corresponding basins of attraction by integrating the differential equation over a time interval $[0, T_1]$, with $T_1 \geq T_0$ still much smaller than the entire time evolution T_f, in such a way that, as a result, the computation time is reduced by a factor T_f/T_1. To do this, a set of initial conditions is chosen and, for each, the equations are integrated for $t \in [0, T_1]$. Then one checks to where the corresponding trajectories have evolved: this can be achieved by using a movement map, as defined in Section 3. The point in phase space which the trajectory occupies at time T_1 is then rounded to the nearest point on the mesh. Provided T_1 is chosen to be a multiple of the forcing period, we know towards which attractor the rounded point moves asymptotically. Repeating this for all initial conditions allows one to estimate the relative areas of the basins of attraction.

To have an idea of the computational gain one can achieve, take the system described by (2.2), with $\gamma(t)$ evolving from $\gamma_i = 0.05$ toward the final value $\gamma_f = 0.02$, so that one can take $T_f = 3000$. For $T_0 = 48\pi$ one can fix $T_1 = T_0$ (as will be discussed in Section 4.2.2): it turns out that simulations for roughly 500 000 initial conditions take under 12 hours to complete, compared with nearly 10 days for the simulations using full time T_f; we refer to Section 4.2 for more details and to Section 6 for further comments. Of course, as pointed out above, the choice $T_f = 3000$ is not optimal. One may choose a different $T_f(\boldsymbol{x})$ for each initial condition $\boldsymbol{x}$, with the requirement that at time $T_f(\boldsymbol{x})$, the trajectory starting from $\boldsymbol{x}$ has reached an attractor. In practice, it can be convenient to sample the trajectory every fixed, integer multiple of 2π, say every 4π, after a fixed transient; then, with the notation (4.1), say for $T_0 = 48\pi$, we find numerically a value $\overline{T}_f \approx 700\pi$. (We are neglecting the additional computational overhead brought about by checking whether the trajectory has reached an attractor). Thus, when integrating over a time T_0, we have a gain $\overline{T}_f/T_0 = 700/48$, which is less than T_f/T_0, but still appreciable (12 hours instead of more than 7 days — a factor of 14); see also the comments at the end of Section 4.2.2. Moreover, one has to take into account that taking a smaller value of γ_i substantially increases both T_f and $\overline{T}_f$, without affecting T_0, so that a much larger gain factor is obtained when smaller values of dissipation are considered.

Roughly, T_1 is the time needed for the trajectories to fall inside the basins of attraction at constant $\gamma = \gamma_f$, so that their evolution from that instant onwards is known. As a matter of fact, the choice of T_1 is the most delicate issue of the analysis and it strongly depends on the system under investigation. From the discussion above, it may seem natural to take T_1 to be the smallest multiple of the forcing period 2π larger than T_0, because then a trajectory which is inside a given basin of attraction at time T_1 will move towards the corresponding attractor. However, error is inevitably introduced when rounding the coordinates of the trajectories at time T_1 to the nearest point in the mesh. In systems where the basins of attraction are sparse the slight change of coordinate during the approximation may cause the results to be inaccurate. As a consequence it is found that in cases

where T_0 is relatively small, or the basins of attraction are increasingly broken and sparse, T_1 must be taken larger than this.

In principle, using a finer mesh reduces the error in the approximation and should cause the results obtained with the method of fast numerical computation described above to tend towards those when the system is fully integrated. In practice this is not always true, especially for systems with high sensitivity to initial conditions. Indeed, in principle, it is even possible that with a coarse mesh the approximation to the point at time T_1 has the same attractor, while with a finer mesh the new, more accurate approximation moves to a different attractor. Moreover there can be compensations which are destroyed by refining the mesh; this is best explained by a simple example. Imagine that there are two initial conditions, one of which should tend to attractor a_1 and the other to attractor a_2, but which, on the contrary, are predicted to tend to attractors a_2 and a_1, respectively: in this case, the two errors cancel. Suppose we then use a finer mesh and the fate of one of the two points is predicted correctly while the other prediction remains incorrect: now the errors do not cancel and the predictions of the relative areas of the basins of attraction will be in error. However, provided that this is a rare occurrence, increasing the number of points on the mesh will in general tend to increase the accuracy.

Since basins of attraction are computed by taking a large but finite discrete set of initial conditions (either on a mesh or uniformly and randomly distributed), an error is always produced by using the fraction of trajectories converging towards a given attractor to estimate the corresponding relative area. The following statistical result gives the confidence interval for results obtained by Monte Carlo simulation; see [27]. If p and $\hat{p}$ are the actual and estimated probability, respectively, of landing in a given basin of attraction, then we have

$$\hat{p} - z_{\alpha/2}\sqrt{\frac{\hat{p}(1-\hat{p})}{N}} < p < \hat{p} + z_{\alpha/2}\sqrt{\frac{\hat{p}(1-\hat{p})}{N}}, \tag{4.2}$$

where N is the sample size (the number of initial conditions used for the simulation); the variable $z_{\alpha/2}$ is the so-called z value, appropriate to a $(1-\alpha)\times 100\%$ confidence interval [27]. A confidence interval of 95% corresponds to $\alpha = 0.05$, and $z_0.025 \approx 1.96$; this results in the error values shown in Table 1. For example if we take $N = 10\,000$ we can see that if an estimated basin of attraction covers 99.5% of the phase space, then we can state with 95% confidence that the actual basin of attraction will be $(99.5 \pm 0.1386)\%$. Similarly, if the estimated basin covers 0.5% of the phase space, the actual basin of attraction will also be $(0.5 \pm 0.1386)\%$; although the error is the same, the error relative to the basin size is much greater for small basins of attraction. Thus when the basins of attraction are small, it is necessary to use more initial conditions. In the forthcoming analysis, the error in the results obtained with the method of fast numerical computation relative to the fully integrated results will be deemed acceptable if it is less than the estimated 95% confidence interval for the relative areas of the basins of attraction.

		N								
		10 000	50 000	100 000	200 000	300 000	400 000	500 000	600 000	1 000 000
$\hat{p}$ (%)	0.5	0.1386	0.0620	0.0438	0.0310	0.0253	0.0219	0.0196	0.0179	0.0139
	1	0.1950	0.0872	0.0617	0.0436	0.0356	0.0308	0.0276	0.0252	0.0195
	2	0.2744	0.1227	0.0868	0.0614	0.0501	0.0434	0.0388	0.0354	0.0274
	3	0.3344	0.1495	0.1057	0.0748	0.0610	0.0529	0.0473	0.0432	0.0334
	4	0.3841	0.1718	0.1215	0.0859	0.0701	0.0607	0.0543	0.0496	0.0384
	5	0.4272	0.1910	0.1351	0.0955	0.0780	0.0675	0.0604	0.0551	0.0427
	10	0.5880	0.2630	0.1859	0.1315	0.1074	0.0930	0.0832	0.0759	0.0588
	15	0.6999	0.3130	0.2213	0.1565	0.1278	0.1107	0.0990	0.0904	0.0700
	20	0.7840	0.3506	0.2479	0.1753	0.1431	0.1240	0.1109	0.1012	0.0784
	30	0.8982	0.4017	0.2840	0.2008	0.1640	0.1420	0.1270	0.1160	0.0898
	40	0.9602	0.4294	0.3036	0.2147	0.1753	0.1518	0.1358	0.1240	0.0960
	50	0.9800	0.4383	0.3099	0.2191	0.1789	0.1550	0.1386	0.1265	0.0980

Table 1: The 95% confidence interval for various relative areas, when using a Monte Carlo approach with N initial conditions, calculated from equation (4.2). This is to be interpreted as follows: if the value in the table is x, then $p \in [\hat{p} - x, \hat{p} + x]$ with 95% confidence. An estimated relative area $\hat{p}$ has the same expected 95% confidence interval as $1 - \hat{p}$, so it is only necessary to consider basins of attraction up to 50%.

4.2 Application to the pendulum with oscillating support

In this section we investigate, in a concrete model, which types of basin of attraction are suitable for our method of fast numerical computation and how to increase the accuracy with respect to the full integrations. We consider the pendulum with oscillating support, see (2.2), with $\gamma(t)$ varying linearly over a time T_0 from the initial value γ_i to the final value γ_f. The reduction in computational time compared with the the full time span $[0, T_f]$ is a result of the smaller integration time T_1. Since $T_1 \geq T_0$, in systems where T_0 is large and comparable with T_f this advantage is lost. However, it was seen in [15] that most changes to the relative areas of the basins of attraction happen over a short initial time T_0, where the method is particularly effective.

The numerical integration schemes used to test the method are: MATLAB's ODE113, which is a variable order Adams-Bashforth-Moulton scheme, and two other integration methods, a standard Runge-Kutta integrator and a scheme based on series expansion [14], both of which were implemented in C. Even though the latter two are expected to be more efficient, we have considered also the integrator ODE113 because MATLAB offers ease in programming compared to using a low-level language such as C. Indeed, our aim is mainly to compare the method of fast numerical computation with the full time integration: taking three different methods confirms that the results are robust with respect to the choice of the numerical integrator. For the same reason, throughout, the relative areas of the basins of attraction are given to 4 decimal places, despite the number of initial conditions for the full simulations producing uncertainty in the first or second decimal place — see Table 1. Moreover, we find that the error produced by the method of fast numerical computation is within the difference produced by simply choosing a different numerical method and a different selection either of initial conditions or of meshes to approximate solutions at time T_1.

To test the method, we consider cases where the basins of attraction for constant values of $\gamma = \gamma_f$ become increasingly sparse. We study (2.2) with $\alpha = 0.5$, $\beta = 0.1$ and $\gamma_f = 0.05$ and 0.02; the corresponding basins of attraction are given in Figures 2(d) and 2(a) in [15], respectively. For $\gamma = 0.02$ the system exhibits four persisting attractors, namely the fixed point $(\theta, \dot{\theta}) = (0, 0)$, two period 1 solutions, one positively rotating and one negatively rotating, and a period 2 solution oscillating around the fixed point; we shall refer to them as FP, PR, NR and OSC, respectively. Further details on these attractors can be found in [28, 15]. For $\gamma = 0.05$, only FP and OSC persist. Similar tests have also been conducted for $\alpha = -0.1$, $\beta = 0.545$ and $\gamma_f = 0.2$, where the basins of attraction are as in Figure 13(a) in [15]. However, owing to the simple geometry of these basins of attraction (they are not intertwined as for the other values of the parameters), in such a case we expected and found perfect agreement between the results obtained with the full simulations and those obtained with the method of fast numerical computation (with $T_1 = T_0$ turning out to be a natural, efficient choice). As such the results have not been presented below. Hence we shall use the parameters $\alpha = 0.5$, $\beta = 0.1$ throughout the rest of this section.

In order to implement the method of fast numerical computation, first a mesh of initial conditions must be set up inside the sample region $[-\pi, \pi] \times [-4, 4]$ and for each of these the equations must be integrated for constant damping γ_f. This is computationally expensive as the system is integrated over the full time span $[0, T_f]$, required for solutions to move sufficiently close to the corresponding attractors that they can be identified. For the chosen values of γ, this yields T_f larger than 10^3. We have considered initial conditions on a mesh (the same as above, for simplicity) for the ODE113 integrator and both initial conditions on the same mesh and random initial conditions for the other two integrators: as the results do not appear to depend on the choice of the initial conditions (within the numerical error), only the results with random initial conditions have been included for the latter two integrators in the tables below.

Another remark, useful for practical purposes, is that using the contracted phase space — see Figure 3 — for our smallest value of T_0, 8π, we can see that it is unnecessary to cover the entire region S with a mesh of initial conditions, as roughly half of them will never be used. Only covering the rectangle that bounds the region $C_{8\pi}$ more tightly, that is roughly $[-\pi, \pi] \times [-2.1, 2.1]$, would reduce both the computation time and memory required by a factor of roughly 2; see Figure 3.

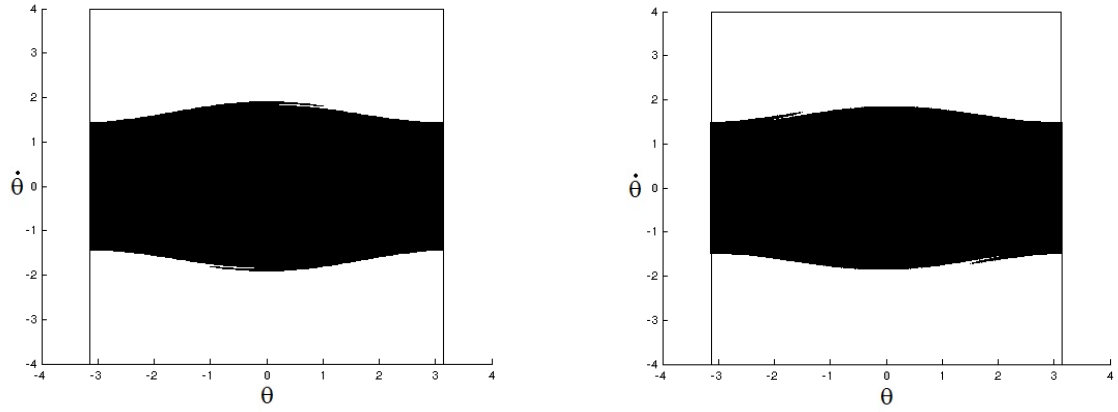

(a) (b)

Figure 3: Contracted phase space for (2.2) $\alpha = 0.5$, $\beta = 0.1$ and $\gamma(t)$ varying linearly over a time $T_0 = 8\pi$ (a) from $\gamma_i = 0.02$ to $\gamma_f = 0.05$ and (b) from $\gamma_i = 0.05$ to $\gamma_f = 0.02$. The rectangle containing the shaded region marks the area S, from which initial conditions were taken.

4.2.1 Two coexisting attractors

We first consider $\gamma(t)$ linearly evolving from 0.02 to 0.05 over a time $T_0 = 2\pi N$, with $N \in \mathbb{N}$, and fix the integration time at $T_1 = T_0$. A mesh of roughly 500 000 points is considered in S and each trajectory at time T_1 is rounded to the nearest point of the mesh. The results in Table 2 show that the method performs well in this instance. Indeed, the error produced by estimating the basins of attraction with the method of fast numerical computation rather than integrating over the full time T_f is less than the difference in results obtained by choosing a different integrator — see Figure 4.

	Relative area %									
	ODE113 Fast		ODE113		Series Fast		Series		Runge-Kutta	
T_0	FP	OSC	FP	OSC	FP	OSC	FP	OSC	FP	OSC
0	N/A	N/A	85.5832	14.4168	N/A	N/A	85.6522	14.3478	85.6744	14.3256
8π	86.1340	13.8660	86.0804	13.9196	86.1818	13.8182	86.1812	13.8188	86.1510	13.8490
16π	86.1977	13.8023	86.1874	13.8126	86.2572	13.7428	86.2370	13.7630	86.1566	13.8434
24π	84.0702	15.9298	84.0855	15.9145	84.1378	15.8622	84.1346	15.8654	84.0230	15.9770
32π	80.4622	19.5378	80.4795	19.5205	80.4374	19.5626	80.4330	19.5670	80.5804	19.4196
48π	75.6663	24.3337	75.6652	24.3348	75.6666	24.3334	75.6776	24.3224	75.6702	24.3298
64π	75.4444	24.5556	75.4472	24.5528	75.4918	24.5082	75.4912	24.5088	75.4440	24.5560
128π	77.3244	22.6756	77.3302	22.6698	75.8202	24.1798	75.8234	24.1766	75.8780	24.1220
160π	77.9221	22.0779	77.9191	22.0809	78.4282	21.5718	78.4280	21.5720	78.4092	21.5908

Table 2: Relative areas of the basins of attraction for (2.2) with $\alpha = 0.5$, $\beta = 0.1$ $\gamma_i = 0.02$, $\gamma_f = 0.05$. Initial conditions for ODE113 were taken from the same mesh (with $\Delta\theta = \Delta\dot{\theta} = 0.01$) as used to approximate trajectories at time T_1, totalling $629 \times 801 = 503\,829$ points. The Runge-Kutta and Series integrators each used different sets of 500 001 random initial conditions in S. The "ODE113 Fast" and "Series Fast" results used the same integrator and the same initial conditions as "ODE113" and "Series", respectively.

By looking at Table 2, one sees that the results obtained with the integrator ODE113 are slightly different from those obtained with the other integrators for $T_0 = 128\pi$ and $T_0 = 160\pi$; nevertheless, in those cases as well, the results obtained with the method of fast numerical computation are still close to the full integrations with the respective integration scheme. This suggests that the method correctly describes the sizes of the basins of attraction, independently of the integrator that is used.

Of course Table 2 allows comparison only of the relative areas of the basins of attraction, but does not reveal to what extent the corresponding sets of points match each other. As pointed out in Section 4.1, there could be substantial compensations and, in principle, the distribution of the basins of attraction in phase space could be wrongly described by the method of fast numerical

computation despite the good agreement between the corresponding relative areas. However, Table 3 shows that this is not the case: it is true that the percentage of points assigned by the method of fast numerical computation to the wrong basin is larger than suggested by Table 2, but still is not large, and also tends to decrease with increasing T_0 and hence T_1.

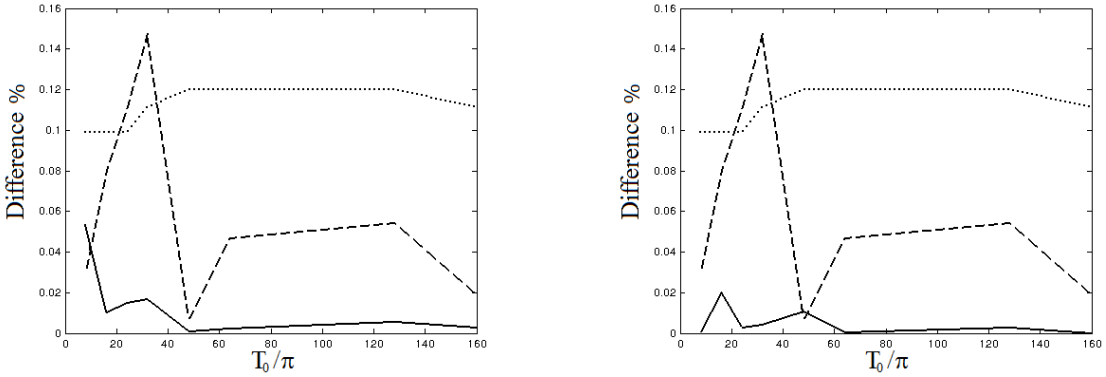

(a) (b)

Figure 4: Error in the relative areas of the basins of attraction in Table 2: (a) difference between "ODE113 Fast" and "ODE113", (b) difference between "Series Fast" and "Series". The full line represents the error of the method of fast numerical computation with respect to the full integration, the dashed line represents the difference between the estimates of "Series" and "Runge-Kutta" and the dotted line represents the 95% confidence interval, as calculated in Section 4.1.

	Accuracy of the method %	
T_0	ODE113 Fast	Series Fast
8π	96.6004	97.1218
16π	99.0513	99.1206
24π	99.6497	99.6984
32π	99.8577	99.8860
48π	99.9464	99.9686
64π	99.9678	99.9922
128π	99.7600	99.9999
160π	99.5254	99.99998

Table 3: The percentages of initial conditions for which the limiting behaviour is correctly described for the simulations in Table 2 using the method of fast numerical computation instead of the full integration.

4.2.2 Four coexisting attractors

The case studied so far may still be regarded as a very simple case, as only two attractors coexist and the boundaries of their basins of attraction for constant γ_f still have relatively simple geometry. We now consider (2.2), with the same values for α and β as in the previous case, but with $\gamma(t)$ linearly decreasing from $\gamma_i = 0.05$ to $\gamma_f = 0.02$.

We first ran simulations with roughly 500 000 initial conditions. We considered two meshes with increments $(\Delta\theta, \Delta\dot{\theta}) = (0.01, 0.01)$ and $(0.005, 0.005)$, respectively: at time $T_1 = T_0$ each trajectory was rounded to the nearest point of the mesh. Afterwards we considered roughly 1 000 000 initial conditions and three meshes with increments $(\Delta\theta, \Delta\dot{\theta}) = (0.01, 0.01)$, $(0.01, 0.005)$ and $(0.005, 0.005)$, respectively, and chose once more $T_1 = T_0$; the corresponding results are reported in Table 4. Figure 5 illustrates that, as previously, the difference between the fast numerical computations and the full time integrations is comparable to — if not smaller than — both the difference between the results obtained with the other two integrators and the 95% confidence interval; note that, for a better visualisation, a logarithmic scale has been used along the vertical axis in Figure 5 (as well as in the forthcoming Figure 7).

		Relative area %					
T_0	Attractor	Fast 1	Fast 2	Fast 3	ODE113	Series	Runge-Kutta
0	FP	N/A	N/A	N/A	71.8847	71.2994	71.3856
	PR	N/A	N/A	N/A	4.6098	4.8996	4.8844
	NR	N/A	N/A	N/A	4.6149	4.8800	4.8916
	OSC	N/A	N/A	N/A	18.8906	18.9210	18.8384
8π	FP	71.9491	72.0382	72.1258	72.0892	71.4668	71.4953
	PR	4.6425	4.6150	4.5799	4.5587	4.8784	4.8529
	NR	4.6513	4.6132	4.5706	4.5540	4.8703	4.8484
	OSC	18.7572	18.7336	18.7237	18.7982	18.7845	18.8034
16π	FP	73.2636	73.3001	73.3398	73.1836	72.6196	72.6889
	PR	4.2390	4.2512	4.2130	4.1818	4.4743	4.4508
	NR	4.2441	4.2515	4.2054	4.1828	4.4691	4.4652
	OSC	18.2533	18.1972	18.2418	18.4518	18.4370	18.3951
24π	FP	76.1441	76.1815	76.2378	76.0930	76.0347	76.0037
	PR	3.1458	3.1531	3.1333	3.1330	3.1620	3.1668
	NR	3.1466	3.1548	3.1281	3.1353	3.1826	3.2077
	OSC	17.5635	17.5105	17.5008	17.6387	17.6207	17.6218
32π	FP	76.9920	77.0224	77.0556	76.9517	76.9123	76.8659
	PR	2.1505	2.1358	2.1274	2.1375	2.0973	2.1022
	NR	2.1416	2.1315	2.1281	2.1363	2.1171	2.1130
	OSC	18.7158	18.7103	18.6888	18.7745	18.8733	18.9189
48π	FP	76.3075	76.3077	76.3121	76.2824	76.2565	76.3226
	PR	0.9210	0.9172	0.9179	0.9176	0.8702	0.8789
	NR	0.9209	0.9169	0.9184	0.9179	0.8750	0.8771
	OSC	21.8505	21.8582	21.8515	21.8820	21.9983	21.9189
64π	FP	77.6648	77.6674	77.6690	77.6652	77.6993	77.7806
	PR	0.2970	0.2971	0.2965	0.2962	0.2752	0.2819
	NR	0.2972	0.2972	0.2968	0.2964	0.2758	0.2739
	OSC	21.7410	21.7383	21.7377	21.7422	21.7497	21.6636
128π	FP	81.0690	81.0690	81.0690	81.0688	81.1812	81.1750
	OSC	18.9310	18.9310	18.9310	18.9312	18.8188	18.8250
160π	FP	81.8492	81.8492	81.8492	81.8491	81.9317	81.9386
	OSC	18.1508	18.1508	18.1508	18.1509	18.0683	18.0614

Table 4: Results for $\gamma(t)$ varying from $\gamma_i = 0.05$ to $\gamma_f = 0.02$ over times T_0. The Runge-Kutta and Series integrators used different sets of 1 000 001 random initial conditions in S, while ODE113 used a mesh of initial conditions in S with increments $(\Delta\theta, \Delta\dot{\theta}) = (0.01, 0.005)$. The meshes in "Fast 1", "Fast 2" and "Fast 3" have increments $(\Delta\theta, \Delta\dot{\theta}) = (0.01, 0.01)$, $(0.01, 0.005)$ and $(0.005, 0.005)$, respectively.

As expected, the difference between the results obtained using different integrators reduces noticeably when increasing the number of initial conditions. Contrary to this, apparently, neither increasing the number of initial conditions nor using a finer mesh in general significantly improves the error relative to the full time integration — see Table 5 for both simulations with roughly 500 000 and 1 000 000 initial conditions. Slight improvements are only obtained for the attractors with smaller basin of attraction (that is the two rotating solutions), where the error becomes comparable to that created by using different numerical integrators and sets of initial conditions.

	Accuracy of the method %				
	$N \approx 500\,000$		$N \approx 1\,000\,000$		
T_0	Mesh 1	Mesh 3	Mesh 1	Mesh 2	Mesh 3
8π	77.1284	77.1986	76.5894	75.8780	78.0587
16π	87.9880	87.9715	88.0697	86.8358	88.7351
24π	95.0983	95.4209	95.0905	93.6584	95.4112
32π	97.4872	97.7471	97.5068	96.3252	97.7284
48π	99.6298	99.6542	99.6308	99.3272	99.6504
64π	99.9637	99.9637	99.9585	99.9262	99.9586
128π	99.9996	99.9996	99.9996	99.9996	99.9996
160π	99.9998	99.9998	99.9999	99.9999	99.9999

Table 5: The percentages of initial conditions for which the limiting behaviour is correctly described for the simulations in Table 4 and the analogous ones with 500 000 initial conditions. Mesh 1, Mesh 2 and Mesh 3 correspond to increments $(\Delta\theta, \Delta\dot{\theta}) = (0.01, 0.01)$, $(0.01, 0.005)$ and $(0.005, 0.005)$, respectively.

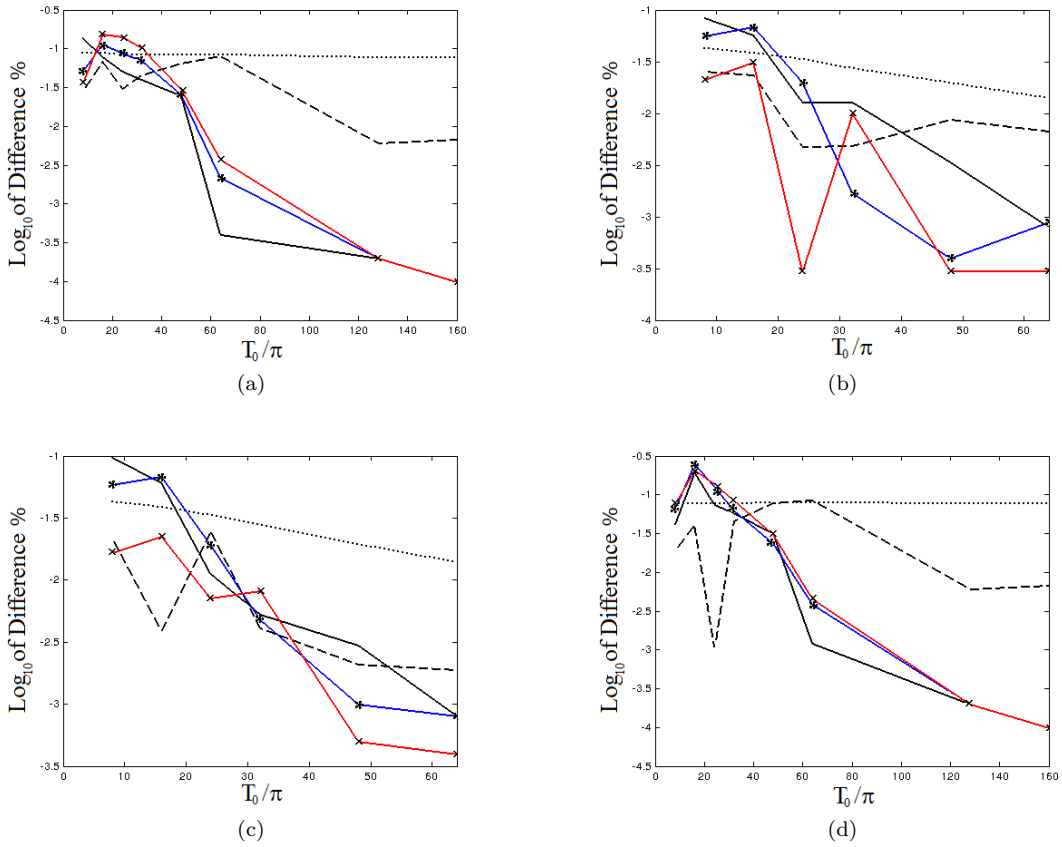

Figure 5: Base-10 logarithm of the error in the relative areas of the basins of attraction in Table 4: Figures (a) through to (d) show the differences for FP, PR, NR and OSC, respectively, with (b) and (c) only going as far as $T_0 = 64\pi$ since the rotating solutions disappear after this. The plain, starred and crossed full lines show the difference between "Fast 1", "Fast 2" and "Fast 3", respectively, and "ODE113". The dashed line shows the difference between the estimates using "Series" and "Runge-Kutta". The dotted line shows the 95% confidence interval.

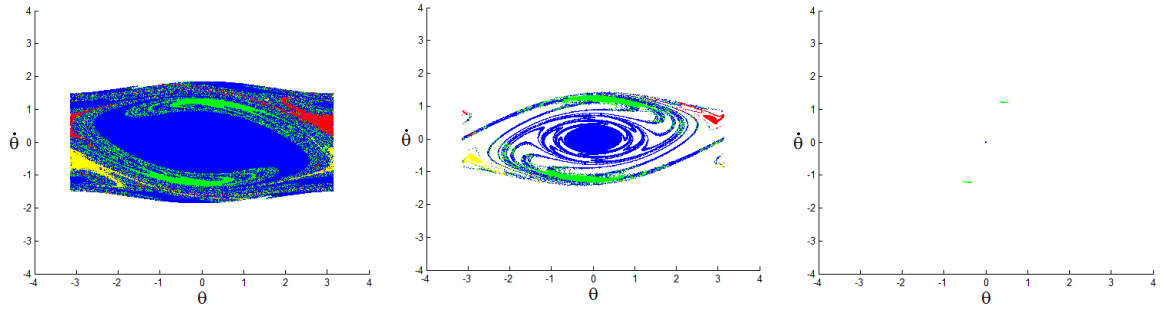

Figure 6: Images of the contracted phase space C_{T_1} superimposed on top of the basins of attraction for constant $\gamma_f = 0.02$. The values of T_1 are (a) 8π, (b) 32π and (c) 160π.

It is also apparent that the larger the value of T_0 (and thus also T_1), the more reliable the method. Table 5 shows that for $T_0 \geq 48\pi$ the results are correct for more than 99% of initial conditions. The reason behind this can be seen by plotting the contracted phase space C_{T_1} for different values of T_1 and superimposing it on the basins of attraction for constant $\gamma = \gamma_f = 0.02$; see Figure 6. When T_1

is larger, C_{T_1} occupies regions of the basin of attraction which are deep inside the cores surrounding the attractors; thus, they are distant from the boundaries and hence less sensitive to slight variations in initial conditions. In turn, the error created by the process of approximation onto the mesh is less significant. For the same reason, as the results in Table 4 corresponding to $T_0 = 128\pi$ and 160π show, decreasing the spacing of points in the mesh does not improve the results for T_0 large.

	Relative area %							
	Fast 1				Fast 3			
T_0	FP	PR	NR	OSC	FP	PR	NR	OSC
8π	72.1750	4.5484	4.5771	18.6995	72.1704	4.5795	4.5661	18.6838
16π	73.2071	4.1834	4.2040	18.4054	73.2283	4.1922	4.1835	18.3960
24π	76.1309	3.1296	3.1390	17.6005	76.1392	3.1359	3.1327	17.5922
32π	76.9679	2.1347	2.1343	18.7631	76.9765	2.1371	2.1350	18.7514

Table 6: Results for $\gamma(t)$ varying from $\gamma_i = 0.05$ to $\gamma_f = 0.02$ over times T_0, with integration time $T_1 = 48\pi$. The meshes for "Fast 1" and "Fast 3" have increments of $(0.01, 0.01)$ and $(0.005, 0.005)$, respectively.

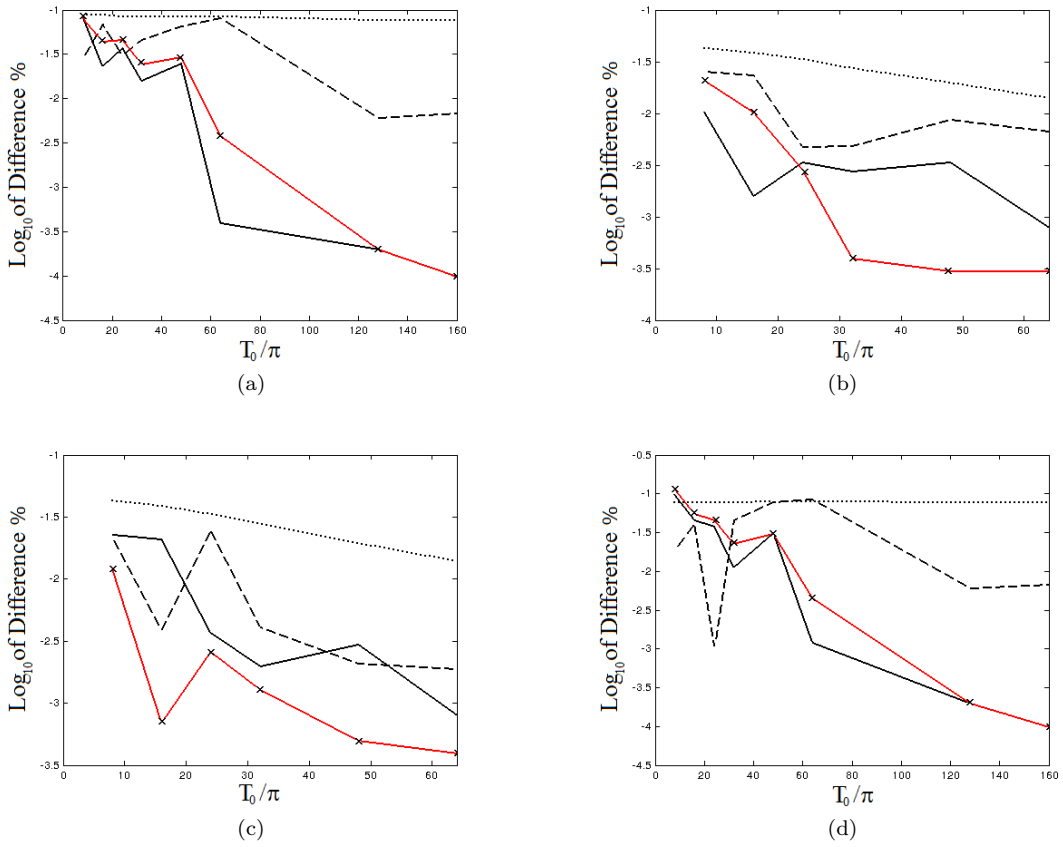

Figure 7: The same as Figure 5 with an integration time $T_1 = \max\{48\pi, T_0\}$. The plain and crossed full lines show the differences between "Fast 1" and "Fast 3", respectively, and "ODE113".

All this suggests that setting a minimum value $T_{\min}$ for the integration time T_1 increases the accuracy of the method of fast numerical computation. Doing so also results in an increase in the computational time if $T_1 \gg T_0$. However it is still quicker than integrating over the full time T_f. Moreover the larger T_1, the less of phase space the mesh is required to cover, so reducing the number of points in the mesh. Tables 6 and 7 give the results, for the relative areas of the basins of attraction and the percentages of initial conditions which are correctly described, obtained by integrating solutions over a time $T_1 = 48\pi$ instead of $T_1 = T_0$, to be compared with those in Table

4 and 5, respectively. Figure 7 shows that the error has dramatically decreased, falling below the differences between the other two integrators, even when a coarse mesh is used (to reduce further the overall integration time). The conclusion is that to optimise the results in such a case one has to fix $T_{\min} = 48\pi$ and choose $T_1 = \max\{T_{\min}, T_0\}$. In general $T_{\min}$ has to be determined case by case — see Section 6 for further comments.

	Accuracy of the method %	
	Fast 1	Fast 3
8π	94.8805	95.1295
16π	96.2629	96.4448
24π	98.0571	98.1563
32π	98.7308	98.8242

Table 7: The percentages of initial conditions for which the limiting behaviour is correctly described for the simulations in Table 6 using an integration time $T_1 = 48\pi$ instead of $T_1 = T_0$. The results are less than 99% accurate because $\gamma_i > \gamma_f$ and hence S contracts more slowly at $\gamma = \gamma_f$, i.e. in the region $[T_0, T_1]$.

If we consider the set of all runs in Table 4, with T_1 chosen as above, and take into account the values of $\overline{T}_f$ (see the definition in (4.1) and the comments thereafter), we find that the overall gain factor is about 10. Indeed, $\overline{T}_f$ has an average value decreasing from 700π to 500π, approximately, when varying T_0 from 24π to 160π. Of course, the gain is slightly reduced with respect to the value 15 found for the run corresponding to $T_0 = 48\pi$, because of the runs with higher values of T_0. However, in practice, the overall integration time is still remarkable: 6 days against 2 months for the straightforward integrations.

5 Jumps in the relative areas of the basins of attraction

We consider (2.2) with $\alpha = -0.1$, $\beta = 0.545$ and $\gamma(t)$ varying from $\gamma_i = 0.23$ to $\gamma_f = 0.2725$. For $\gamma = \gamma_i$ the system possesses four attractors: the fixed point (FP), the period-1 positively and negatively rotating solutions (PR/NR) and the period-2 oscillations (DO2); for $\gamma = \gamma_f$ only FP and DO2 survive and a new attractor appears: the period-4 oscillation (DO4) — we refer to [15] for more details. The corresponding basins of attraction are shown in Figures 13(b) and 13(a) in [15], respectively. In Figure 8 the basins of attraction when $\gamma(t)$ varies in time from $\gamma_i = 0.23$ to $\gamma_f = 0.2725$ are represented for a few values of T_0.

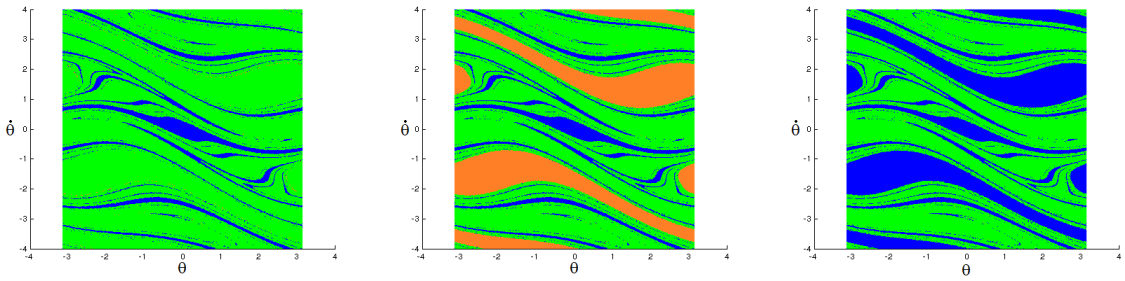

(a) (b) (c)

Figure 8: Basins of attraction for (2.2) with $\alpha = -0.1$, $\beta = 0.545$ and $\gamma(t)$ increasing linearly from $\gamma_i = 0.23$ to $\gamma_f = 0.2725$ over a time (a) $T_0 = 93.6$, (b) 94.0 and (c) 99.2. The basins are coloured as follows: Blue = FP, Green = DO2, Red=PR, Yellow=NR, Orange = DO4.

In [15], for $\gamma(t)$ varying from $\gamma_i = 0.23$ to $\gamma_f = 0.2725$ over a time T_0, we noticed large transitions in the basins of attraction for $T_0 = 99$, 100, 500; see Figure 22 in [15]. To understand why a jump appears, say, for $T_0 = 99$, we can reason as follows. We increase T_0 in steps of one from 92 to 99. For all such values the appropriate density map shows that, after a time $T_1 = 32\pi > T_0$, over 90% of the trajectories are clustered in very small regions — see Figure 9(a). This is an effect of the

dissipation being rather large. Indeed, all trajectories start tending to the attractors existing at $\gamma = 0.23$. However, with the dissipation changing, also the attractors change quasi-statically. The attractors FP and DO2 still persist at $\gamma = 0.2725$. Most of the trajectories moving towards them form clusters at time T_1 close to the points at which the attractors cross the plane at $t = T_1$; we denote by FP and DO2 such clusters, according to the attractor they are approaching. Instead, the attractors PR and NR disappear when the damping coefficient reaches the value $\gamma \approx 0.269$ [15]. The trajectories that were moving towards them form clusters that we denote by U. Thus, at time T_1, there are seven clusters of points: two clusters U, one cluster FP and four clusters DO2 (since up to $\gamma \approx 0.27$ there are two period-2 solutions) — see Figure 9. The cluster FP and each cluster DO2 correspond roughly to 20% and 11–13% of initial conditions, respectively, while the two clusters U each represent roughly 12% of the initial conditions (approximately the relative areas of the basins of attraction for the rotating solutions at $\gamma = 0.23$).

Since both attractors FP and DO2 remain stable for all values of $\gamma \in [\gamma_i, \gamma_f]$, it is unlikely that the clusters labelled as FP and DO2 will change their limiting solutions. This is confirmed by the fact that the clusters FP and DO2 are well inside the basins of attraction of the corresponding attractors FP and DO2, respectively, for all values of T_0. On the contrary the clusters U move slightly from right to left in the upper half-plane and from left to right in the lower half-plane as T_0 increases. In doing so, they cross the boundaries of the basins of attraction for constant $\gamma = 0.2725$.

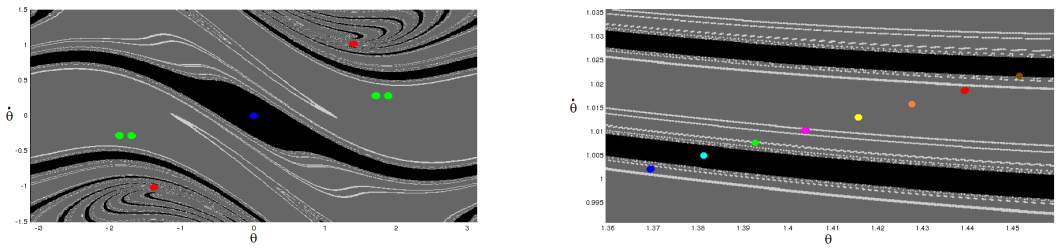

(a) (b)

Figure 9: Clusters into which 90% of the initial conditions have evolved after a time $T_1 = 32\pi$. The clusters are superimposed onto basins of attraction for constant $\gamma = 0.2725$: (a) whole sample region with clusters FP, DO2 and U in Blue, Green and Red, respectively, and (b) magnification of the region containing the clusters U in the upper half-plane (here the colour code is: Blue = 92, Cyan = 93, Green = 94, Magenta = 95, Yellow = 96, Orange = 97, Red = 98, Brown = 99). The basins are colour coded with Black for FP, Dark Grey for DO2 and Light Grey for DO4. The coloured dots have been drawn larger than the actual sizes of the clusters for clarity purposes.

We interpret the results above as follows. After some transient behaviour, the original sample phase space has contracted enough and been re-organised so that some regions of phase space become more dense than others; in particular most of the trajectories end up inside some small, well separated clusters. The clusters U were converging towards the attractors PR/NR; however, because of the different evolution of $\gamma(t)$, they occupy slightly different positions at time T_1 as T_0 is varied. Since they fall in a region where the basins of attraction for $\gamma = 0.2725$ are sparse and formed of very thin bands, changing the value of T_0 may cause the clusters to cross the boundaries separating the bands belonging to different basins — see Figure 9(b). This results in a large jump in the relative area of the basin of attraction of FP, as shown in Figures 21 and 22 in [15]; see also Figure 8. According to the results reported in Figure 10, the clusters U fall inside the basin of attraction of FP for $T_0 = 93$ and 99, inside the basin of attraction of DO2 for $T_0 = 92$, 95, 96, 97 and 98, and inside the basin of attraction of DO4 for $T_0 = 94$.

We expect the jumps to occur for many other values of T_0. Figure 10 shows that jumps upward take place for FP, for instance, at $T_0 \approx 72.6$, 79.2, 85.8, 92.4, 99.0 and 105.6. When a peak appears, it survives for a very narrow range of T_0 (proportional to the width of the bands of the basins of attraction), after which a jump downward follows. For this reason, in practice it is difficult to predict

exactly the values of T_0 where jumps occur, even though apparently they follow an approximately periodic pattern — at least in the range of values that we have investigated. Indeed, every value of T_0 at which a jump appears is obtained by adding approximately the same quantity $\Delta T_0 \approx 6.6$ to the previous one. For some values of T_0 the basin of attraction of the period-4 oscillation has grown, which implies that the basin of attraction of the new attractor DO4 has formed exactly where the dense region U has arrived at that time. Also in the case of DO2 and DO4 the jumps seem to have some periodicity in T_0, however with a more intricate structure. It would be interesting to investigate further such a phenomenon.

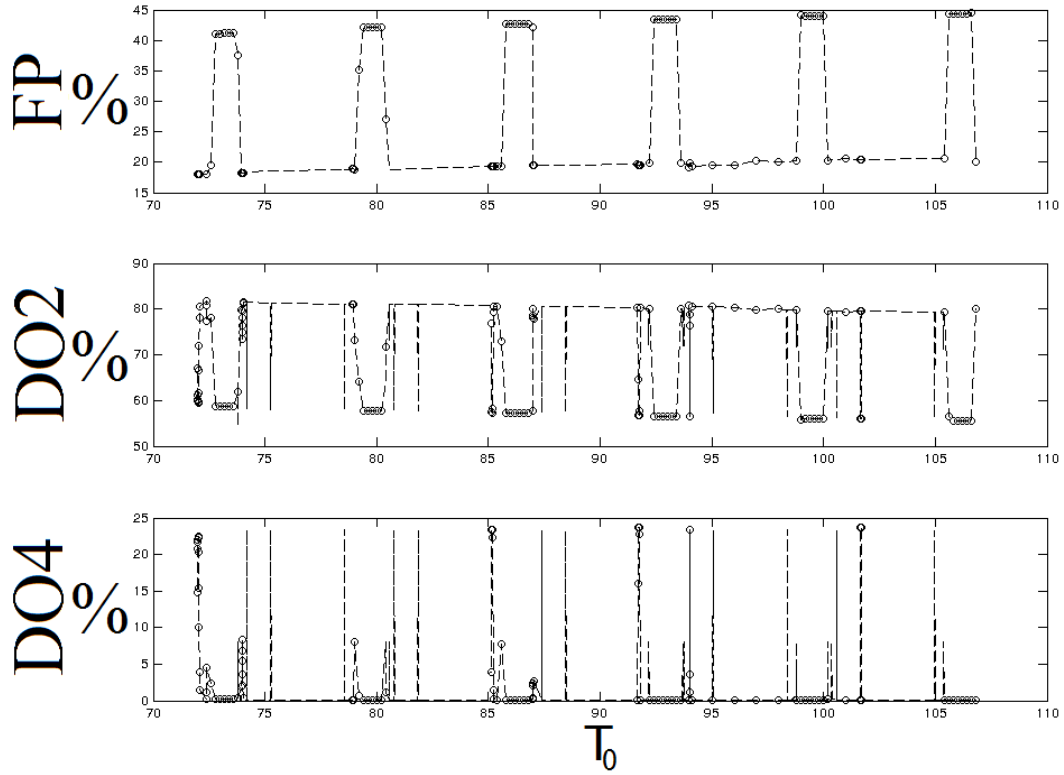

Figure 10: Relative areas of the basins of attraction for (2.2) with $\alpha = -0.1$, $\beta = 0.545$ and $\gamma(t)$ varying from $\gamma_i = 0.02$ to $\gamma_f = 0.05$ over a time T_0. The circles represent results from numerical simulation, while the dashed lines are extrapolated on the basis of the observed periodicity — see the text for details.

Note that, if one applies the method of fast numerical computation described in Section 3 to compute the relative areas of the basins of attraction in these cases, one needs to take either a much larger value for the time T_1 at which the trajectories are approximated to the closest points of the mesh, or a much finer mesh. More generally, this happens every time (i) an attractor disappears with increasing dissipation and (ii) the trajectories which were moving towards that attractor cluster into a small set in a region with narrow bands of the basins of attraction for $\gamma = \gamma_f$. Then, if the mesh is fixed, T_1 must be large enough for the clusters to have reached the core surrounding some persisting attractor. Indeed, if at the observation time T_1 the clusters (which have finite size) touch or even spread across the boundaries of the bands, then the approximation with the points of the mesh introduces too many errors. Therefore, T_1 must be very large for the method of fast numerical integration to work, in principle as large as T_f itself. In this case the method may have no advantage over full time integration of the equations. However, another possibility is to decrease the step of the mesh, so as to make it smaller than the width of the thin bands of the basins of attraction. Of course, what is gained by taking a smaller value of T_1 is lost by increasing the number of initial conditions on the mesh. However, this has to be done only once (when computing the basins of attraction

for constant damping coefficient γ_f) and, moreover, one can consider only initial conditions in a subregion of phase space (see the comment immediately before Section 4.2.1).

In practice, the choice of T_1 has to be decided on a case by case basis. The situation is easier for values of the parameters in the perturbation regime, where explicit analytical computations can be performed to determine the coexisting attractors [15] (see also [29, 30, 31] for a different approach). In particular one can predict whether some attractors disappear during the time evolution of the dissipation, by explicitly calculating the threshold values above which the attractors no longer exist [32, 15] (see also [26, 7, 14] for other models within the class we have considered in this paper). If this happens, one can look at the basins of attraction for $\gamma = \gamma_f$ and choose T_1 large enough for the trajectories to fall well inside the basins after that time. If on the contrary no attractors disappear, a much smaller value of T_1 can be taken. Far away from the perturbation regime, the numerical analysis is expected to be harder, because there are no analytical results available to rely upon and the determination of T_1 in general requires more care — see also the comments in Section 4.2.2.

6 Conclusions

The method of fast numerical computation can be used to estimate the basins of attraction in forced systems with damping coefficient $\gamma(t)$ varying linearly between two given values γ_i and γ_f over a time T_0. First, one fixes a mesh of points in phase space and, for each, one computes which basin of attraction it belongs to when the damping coefficient is constant and equals γ_f, integrating the equation up to a long time T_f. Then one considers the system with varying dissipation: one integrates the equations over a time interval $[0, T_1]$ for a large set of initial data and then approximates each trajectory at time T_1 with the closest point of the mesh. If T_1 can be taken much smaller than T_f, the computational time can be reduced significantly — up to a factor 20 in some cases we considered.

The method works well for systems which have at least some regions surrounding the persisting attractors which are not sensitive to slight perturbations in initial conditions. It becomes more accurate as the integration time T_1 increases, a result of the phase space contracting into regions distant from the boundaries of the basins of attraction. Thus the results can be improved by setting a minimum time $T_{\min}$, and taking $T_1 = 2\pi N \geq \max\{T_0, T_{\min}\}$ (if 2π is the period of the forcing). This seems to be necessary when T_0 is rather small or such that an attractor disappears in a region where the basins of attraction of the persistent attractors have a multi-band structure.

Of course, it is not easy to fix $T_{\min}$. This strongly depends on the model and cannot be prescribed by giving a universal rule. On the contrary, one has to proceed on a case-by-case basis: $T_{\min}$ has to be considered as a parameter and one should try to fix it in order to optimise the computational time. On the one hand this is somewhat unsatisfactory because one cannot decide *a priori* the value of the parameter; on the other hand it is not unusual, in problems of numerical analysis, for there to be free parameters that one has to adjust by hand. So, a practical criterion could be to compare the full integrations with the results obtained through the method of fast numerical computation for several values of $T_{\min}$ and then choose the minimal value of $T_{\min}$ for which the two results match within the numerical error. As a guideline, one should bear in mind that the smaller γ_f is, the larger the value of $T_{\min}$ one should expect to take. In particular, if the basins of attraction are so sparse that no appreciable open regions can be found around the attractors (a situation which can arise when a large number of attractors coexist [16]), we do not expect that the method can be profitably used in order to reduce the computational time. On the contrary, if the basins of attraction have an open core around the attractors, as in the cases studied in the paper and in the literature quoted in Section 1, it is possible to choose $T_{\min}$ properly, possibly after several attempts, so as to apply the method.

Using a finer mesh does not necessarily improve the results. One can imagine that, if the basins of attraction are not too sparse, there is a threshold beyond which increasing the mesh increments does not improve the results. However, smaller basins of attraction benefit from a finer mesh. Indeed, they intersect only a few points of the mesh and hence, if a coarse mesh is used, inaccurate predictions become more likely. In the case that the basins of attraction are very sparse and with

very narrow bands, using a very fine mesh seems to be mandatory — see comments in Section 5. The accuracy could be improved further by using a mesh with non-uniform spacing and better fitting the mesh to the region C_{T_1} to which the sample phase space has contracted at time T_1. This was not implemented here, as it would add extra numerical complexities when rounding a trajectory at time T_1 to the nearest point on the mesh. Both measures would reduce unnecessary full time integration of initial conditions on the mesh. Further work could be carried out to remove the use of a mesh and instead have a set of random initial conditions. Similarly the density of the random initial conditions in particular regions could be chosen so as to optimise the results.

When the dissipation becomes large, at time T_1 the sample region has contracted into very small clusters. If this happens, a very fine mesh is needed for the method to produce accurate results. Essentially, the size of the mesh has to be at least comparable with the sizes of the clusters. For instance, to detect reliably the jumps that may occur in such a case, when an attractor is destroyed while the damping coefficient increases in time, too rough an approximation of the trajectories at time T_1 would produce a completely wrong description of the dynamics. Note, however, that if the dissipation is large, then the convergence to the attractor is fast, so that there is a less pressing need to speed up the computations in that case.

Finally, we note that, even though we have considered explicitly in this paper a case where dissipation varies linearly in time, both for simplicity and for comparison with the literature, we expect our results to extend to more general situations, where the damping depends on time and either becomes constant after a finite time or tends asymptotically to a constant value.

Acknowledgements. The integrator ODE113 is one of the built-in ODE solvers in MATLAB. This research was completed as part of an EPSRC funded PhD. We thank an anonymous reviewer for invaluable comments which allowed us to improve the presentation of the paper.

References

[1] A. Brandon, *A younger moon*, Nature **450** (2007), 1169-1170.

[2] A. Nemchin, N. Timms, R. Pidgeon, T. Geisler, S. Reddy, and C. Meyer, *Timing of crystallisation of the lunar magma ocean constrained by the oldest zircon*, Nature Geosci. **2** (2009), 133-136.

[3] D. L. Turcotte, *On the thermal evolution of the Earth*, Earth Planet. Sci. Lett. **48** (1980), 53-58.

[4] P. Warren, *The lunar magma ocean concept and lunar evolution*, Ann. Rev. Earth Planet Sci. **13** (1985), 201-240.

[5] C. K. Shearer et al., *Thermal and magmatic evolution of the Moon*, Rev. Mineral. Geochem. **60** (2006), 365-518.

[6] S. M. Brown, L. T. Elkins-Tanton, *Compositions of Mercurys earliest crust from magma ocean models*, Earth Planet. Sci. Lett. *286* (2009), 446-455.

[7] M.V. Bartuccelli, J.H.B. Deane, G. Gentile, *Attractiveness of periodic orbits in parametrically forced systems with time-increasing friction*, J. Math. Phys. **53** (2012), no. 10, 102703, 27 pp.

[8] P. Goldreich, S. Peale, *Spin-orbit coupling in the solar system*, Astron. J. **71** (1966), no. 6, 425-438.

[9] C.D. Murray, S.F. Dermott, *Solar System Dynamics*, Cambridge University Press, Cambridge, 1999.

[10] A.C.M. Correia, J. Laskar, *Mercurys capture into the 3/2 spinorbit resonance as a result of its chaotic dynamics*, Nature **429** (2004), 848-850.

[11] B. Noyelles, J. Frouard, V.V. Makarov, M. Efroimsky, *Spin-orbit evolution of Mercury revisited*, Icarus. **241** (2014), 26-44.

[12] E. Y. Aleshkina, *Synchronous spin-orbital resonance locking of large planetary satellites*, Solar Syst. Res. **43** (2009), no. 1, 71-78.

[13] A. Celletti, L. Chierchia, *Measures of basins of attraction in spinorbit dynamics*, Celest. Mech. Dyn. Astron. **101** (2008), no. 1-2, 159-170.

[14] M.V. Bartuccelli, J.H.B. Deane, G. Gentile, *The high-order Euler method and the spin-orbit model*, Celest. Mech. Dyn. Astron. **121** (2015), no. 3, 233-260.

[15] J.A. Wright, M.V. Bartuccelli, G. Gentile, *The effects of time-dependent dissipation on the basins of attraction for the pendulum with oscillating support*, Nonlinear Dynam. **77** (2014), no. 4, 1377-1409.

[16] U. Feudel, C. Grebogi, B.R. Hunt, J.A. Yorke, *Map with more than 100 coexisting low-period periodic attractors*, Phys. Rev E **54** (1996), 71-81.

[17] Ch.S. Rodrigues, A.P.S. de Moura, C. Grebogi, *Emerging attractors and the transition from dissipative to conservative dynamics*, Phys. Rev. E **80** (2009), no. 2, 026205, 8 pp.

[18] J. Palis, *A global view of dynamics and a conjecture on the denseness of finitude of attractors*, Astérisque **261** (2000), 339-351.

[19] W.K. Lee, C.H. Hsu, *A global analysis of an harmonically excited spring-pendulum system with internal resonance*, J. Sound Vibration **171** (1994), no. 3, 335-359.

[20] S.L.T. de Souza, I.L. Caldas, R.L. Viana, J.M. Balthazar, R.M.L.R.F. Brasil, *Basins of attraction changes by amplitude constraining of oscillators with limited power supply*, Chaos Solitons Fractals **26** (2005), no. 4, 1211-1220.

[21] A. Alasty, R. Shabani, *Chaotic motions and fractal basin boundaries in spring-pendulum system*, Nonlinear Anal. Real World Appl. **7** (2006), no. 1, 81-95.

[22] T.J. Kalvouridis, M. Ch. Gousidou-Koutita, *Basins of attraction in the Copenhagen problem where the primaries are magnetic dipoles*, Applied Mathematics and Computation Appl. Math. Comput. **3**, (2012), no. 6, 541-548.

[23] G. Litak, M. Coccolo, M.I. Friswell, Sh.F. Ali, S. Adhikari, A.W. Lees, O. Bilgen, *Nonlinear oscillations of an elastic inverted pendulum*, 4th IEEE Nonlinear Science and Complexity (NSC), Budapest, Hungary, 2012, 113-116.

[24] A.O. Belyakov, A.P. Seyranian, *Dynamics of a pendulum of variable length and similar problems*, Chapter 4 in the book *Nonlinearity, bifurcation and chaos: theory and applications*, Eds. J. Awrejcewicz and P. Hagedorn, INTECH, Rijeka, 2012.

[25] S.R. Bishop, U. Galvanetto *The influence of ramped forcing on safe basins in a mechanical oscillator*, Dynam. Stability Systems **8** (1993), no. 2, 73-80.

[26] M. V. Bartuccelli, A. Berretti, J. H. B. Deane, G. Gentile, S. Gourley, *Periodic orbits and scaling laws for a driven damped quartic oscillator*, Nonlinear Anal. Real World Appl. **9** (2008), no. 5, 1966-1988.

[27] R.H. Myers, S.L. Myers, R.E. Walpole, *Probability and statistics for engineers and scientists*, Sixth edition, Prentice Hall, London, 1998.

[28] M.V. Bartuccelli, G. Gentile, K.V. Georgiou, *On the dynamics of a vertically driven damped planar pendulum*, R. Soc. Lond. Proc. Ser. A Math. Phys. Eng. Sci **457** (2001), no. 2016, 3007-3022.

[29] X. Xu, M. Wiercigroch, *Rotating orbits of a parametrically-excited pendulum* Chaos Solitons Fractals **23** (2005), 1537-1548.

[30] X. Xu, M. Wiercigroch, *Approximate analytical solutions for oscillatory and rotational motion of a parametric pendulum*, Nonlinear Dynam. **47** (2007), no. 1-3, 311-320.

[31] S. Lenci, E. Pavlovskaia, C. Rega, M. Wiercigroch, *Rotating solutions and stability of parametric pendulum by perturbation theory*, J. Sound Vibration **310** (2008), 243-259.

[32] S. N. Chow, J. K. Hale, *Methods of bifurcation theory*, Springer, New York, 1982.